

Article

Jet Transport Coefficient at the Large Hadron Collider Energies in a Color String Percolation Approach [†]

Aditya Nath Mishra ¹, Dushmanta Sahu ² and Raghunath Sahoo ^{2,3,*}

¹ Wigner Research Centre for Physics, 29-33 Konkoly-Thege Miklós Str., 1121 Budapest, Hungary; aditya.nath.mishra@cern.ch

² Department of Physics, Indian Institute of Technology Indore, Simrol, Indore 453552, India; dushmanta.sahu@cern.ch

³ European Organization for Nuclear Research (CERN), CH 1211 Geneva, Switzerland

* Correspondence: raghunath.sahoo@cern.ch

[†] This paper is dedicated to the loving memory of Professor Jean Cleymans, a teacher, collaborator, an excellent human being and a great source of inspiration.

Abstract: Within the color string percolation model (CSPM), jet transport coefficient, \hat{q} , is calculated for various multiplicity classes in proton-proton and centrality classes in nucleus-nucleus collisions at the Large Hadron Collider energies for a better understanding of the matter formed in ultra-relativistic collisions. \hat{q} is studied as a function of final state charged particle multiplicity (pseudorapidity density at midrapidity), initial state percolation temperature and energy density. The CSPM results are then compared with different theoretical calculations from the JET Collaboration those incorporate particle energy loss in the medium.

Keywords: jet quenching; color string percolation; quark-gluon plasma



Citation: Mishra, A.N.; Sahu, D.; Sahoo, R. Jet Transport Coefficient at the Large Hadron Collider Energies in a Color String Percolation Approach. *Physics* **2022**, *4*, 315–328. <https://doi.org/10.3390/physics4010022>

Received: 12 January 2022

Accepted: 23 February 2022

Published: 16 March 2022

Publisher's Note: MDPI stays neutral with regard to jurisdictional claims in published maps and institutional affiliations.



Copyright: © 2022 by the authors. Licensee MDPI, Basel, Switzerland. This article is an open access article distributed under the terms and conditions of the Creative Commons Attribution (CC BY) license (<https://creativecommons.org/licenses/by/4.0/>).

1. Introduction

The main objective of tera-electron volt energy heavy-ion collisions is to form a quark-gluon plasma (QGP)—the deconfined state of quarks and gluons, by creating extreme conditions of temperature and/or energy density [1,2], a scenario that might have been the case after a few microseconds of the creation of the universe. Jets, collimated emission of a multitude of hadrons originating from the hard partonic scatterings, play an important role as hard probes of QGP. These hard jets lose their energy through medium-induced gluon radiation and collisional energy loss, as a consequence of which one observes suppression of high transverse momentum particles and the phenomenon is known as jet quenching [3–9]. This is a direct signature of a highly dense partonic medium, usually formed in high energy heavy-ion collisions. The first evidence of the jet quenching phenomenon has been observed at the Relativistic Heavy-Ion Collider (RHIC) [10–23] via the measurement of inclusive hadron and jet production at high transverse momentum (p_T), γ -hadron correlation, di-hadron angular correlations and the dijet energy imbalance. The jet quenching phenomena are also widely studied in heavy-ion collisions at the Large Hadron Collider (LHC) [24–38]. All the measured observables are found to be strongly modified in central heavy-ion collisions relative to minimum bias proton-proton collisions, when compared to expectations based on treating heavy-ion collisions as an incoherent superposition of independent nucleon-nucleon collisions.

A number of theoretical models that incorporate parton energy loss have been proposed to study the observed jet quenching phenomena, namely, Baier–Dokshitzer–Mueller–Peigne–Schiff–Zakharov (BDMPS-Z) [7,39,40], Gyulassy–Levai–Vitev (GLV) [41–43] and its CUJET implementation [44], high-twist (HT) approach (HT-M (Majumder) and HT-BW (Berkeley–Wuhan)) [45–49], Amesto–Salgado–Wiedemann (ASW) [50,51], Arnold–Moore–Yaffe (AMY) model [52,53], MARTINI model [54], BAMPS model [55], and linear Boltzmann transport (LBT) model [56]. Most of the theoretical models assumed a static potential

for jet-medium interactions, which result in a factorized dependence of parton energy loss on the jet transport coefficient, \hat{q} . The coefficient, which describes the average transverse momentum square transferred from the traversing parton per unit mean free path, is a common parameter that modulates the energy loss of jets in a strongly-interacting quantum chromodynamics (QCD) medium [7,9]. \hat{q} is also related to the gluon distribution density of the medium and therefore characterizes the medium property as probed by an energetic jet [7,57]. Thus the collision energy and system size dependence study of jet transport coefficient will not only improve our understanding of experimental results on jet quenching but also can directly provide some information about the internal structure of the hot and dense QCD matter [57,58].

In the present paper, \hat{q} and its relation with various thermodynamic properties of the QCD matter are studied in the framework of the color string percolation model (CSPM) [59–64] which is inspired by QCD. This can be used as an alternative approach to color glass condensate (CGC) [64] and is related to the Glasma approach [65]. In CSPM, it is assumed that color strings are stretched between the projectile and the target, which may decay into new strings via $q\bar{q}$ pair production and subsequently hadronize to produce observed hadrons [66]. These color strings may be viewed as small discs in the transverse plane filled with color field created by colliding partons. The final state particles are produced by the Schwinger mechanism, emitting $q\bar{q}$ pairs in this field [67]. With the increasing collision energy and size of the colliding nuclei, the number of strings grows and they start interacting to form clusters in the transverse plane. This process is very much similar to discs in the 2-dimensional percolation theory [60,62,68,69]. At a certain critical density, called critical percolation density ($\xi_c \geq 1.2$), a macroscopic cluster appears that marks the percolation phase transition [60,62,68–71]. The combination of the string density dependent cluster formation and the 2-dimensional percolation clustering phase transition are the basic elements of the non-perturbative CSPM. In CSPM, the Schwinger barrier penetration mechanism for particle production and the fluctuations in the associated string tension due to the strong string interactions make it possible to define a temperature. The critical density of percolation is related to the effective critical temperature and thus percolation may provide information on deconfinement in the high-energy collisions [63,64]. The CSPM approach has been successfully used to describe the initial stages in the soft region in high-energy collisions [59,64,68,72–77]. In addition to this, CSPM has also been quite successful in estimating various thermodynamic and transport properties of the matter formed in ultra-relativistic energies [78–84].

The paper runs as follows. Section 2 presents the formulation and methodology of the CSPM approach. Section 3 presents the results and discussions. Finally, the important findings of this study are summarized in Section 4.

2. Formulation and Methodology

In the CSPM, the charged hadron multiplicity, μ_n , where n stands for the number of strings in a cluster, reduces with the increase of string interactions while the mean of the squared transverse momentum, $\langle p_T^2 \rangle_n$, of these charged hadrons increases, to conserve the total transverse momentum. The μ_n and the $\langle p_T^2 \rangle_n$ of the particles produced by a cluster are proportional to the color charge and color field, respectively [62,64], and can be defined as

$$\mu_n = \sqrt{\frac{nS_n}{S_1}} \mu_1; \quad \langle p_T^2 \rangle_n = \sqrt{\frac{nS_1}{S_n}} \langle p_T^2 \rangle_1, \quad (1)$$

where S_n denotes the transverse overlap area of a cluster of n -strings and the subscript '1' refers to a single string with a transverse overlap area $S_1 = \pi r_0^2$ with the string radius, $r_0 = 0.2$ fm [64], respectively. For the case when strings are just touching each other $S_n = nS_1$, and $\mu_n = n\mu_1$, $\langle p_T^2 \rangle_n = \langle p_T^2 \rangle_1$. When strings fully overlap $S_n = S_1$ and therefore $\mu_n = \sqrt{n}\mu_1$ and $\langle p_T^2 \rangle_n = \sqrt{n}\langle p_T^2 \rangle_1$, so that the multiplicity is maximally suppressed and the $\langle p_T^2 \rangle_n$ is maximally enhanced. This implies a simple relation between the multiplicity and transverse momentum $\mu_n \langle p_T^2 \rangle_n = n\mu_1 \langle p_T^2 \rangle_1$, which denotes the conservation of the

total transverse momentum. In the thermodynamic limit, one can obtain the average value of nS_1/S_n for all the clusters [60,62] as

$$\left\langle \frac{n S_1}{S_n} \right\rangle = \frac{\xi}{1 - e^{-\xi}} \equiv \frac{1}{F(\xi)^2}. \tag{2}$$

Here, $F(\xi)$ is the color suppression factor by which the overlapping strings reduce the net-color charge of the strings. With $F(\xi) \rightarrow 1$ as $\xi \rightarrow 0$ and $F(\xi) \rightarrow 0$ as $\xi \rightarrow \infty$, where $\xi = N_s S_1/S_N$ is the percolation density parameter. Equation (1) can be written as $\mu_n = nF(\xi)\mu_1$ and $\langle p_T^2 \rangle_n = \langle p_T^2 \rangle_1/F(\xi)$. It is worth noting that CSPM is a saturation model, similar to the CGC, where $\langle p_T^2 \rangle_1/F(\xi)$ plays the same role as the saturation momentum scale Q_s^2 in the CGC model [65,85].

In the present study, $F(\xi)$ in proton-proton (pp) collisions at the center-of-mass energies $\sqrt{s} = 5.02$ and 13 TeV is extracted for various multiplicity classes using ALICE experiment results on transverse momentum spectra of charged particles [86]. In case of Pb-Pb collisions at the nucleon-nucleon center-of-mass energies $\sqrt{s_{NN}} = 2.76$ and 5.02 TeV [87] and Xe-Xe collisions at $\sqrt{s_{NN}} = 5.44$ TeV [88], $F(\xi)$ values are obtained from the centrality-dependent transverse-momentum spectra of charged particles measured by ALICE. To evaluate the initial value of $F(\xi)$ from data, a parameterization [68] of the experimental data of p_T distribution in low-energy pp collisions at $\sqrt{s} = 200$ GeV (minimum bias), where strings have very low overlap probability, is used. The p_T spectrum of charged particles can be described by a power-law [64]:

$$\frac{d^2 N_{ch}}{dp_T^2} = \frac{a}{(p_0 + p_T)^\alpha}, \tag{3}$$

where a is the normalisation factor and p_0, α are fitting parameters given as, $p_0 = 1.98$ and $\alpha = 12.87$ [64]. This parameterization is used in high-multiplicity pp and centrality-dependent heavy-ion (AA) collisions to take into account the interactions of the strings [64]. The parameter p_0 in Equation (3) is for independent strings and gets modified to

$$p_0 \rightarrow p_0 \left(\frac{\langle nS_1/S_n \rangle^{mod}}{\langle nS_1/S_n \rangle_{pp}} \right)^{1/4}. \tag{4}$$

Using Equations (4) and (2) in Equation (3), one gets:

$$\frac{d^2 N_{ch}}{dp_T^2} = \frac{a}{(p_0 \sqrt{F(\xi)_{pp}/F(\xi)^{mod}} + p_T)^\alpha}, \tag{5}$$

where $F(\xi)^{mod}$ is the modified color suppression factor and is used in extracting $F(\xi)$ both in pp and AA collisions. The spectra were fitted using Equation (5) in the softer sector with p_T in the range 0.15–1.0 GeV/ c , where c is the speed of light. In pp collisions at low energies, only two strings are considered to exchange with low probability of interactions, so that $\langle nS_1/S_n \rangle_{pp} \approx 1$, which transforms Equation (5) into

$$\frac{d^2 N_{ch}}{dp_T^2} = \frac{a}{(p_0 \sqrt{1/F(\xi)^{mod}} + p_T)^\alpha}. \tag{6}$$

In the thermodynamic limit, the color suppression factor $F(\xi)$ is related to the percolation density parameter, ξ , as

$$F(\xi) = \sqrt{\frac{1 - e^{-\xi}}{\xi}}. \tag{7}$$

3. Results and Discussion

In the present study, $F(\xi)$ is extracted in the multiplicity-dependent pp collisions at $\sqrt{s} = 5.02$ and 13 TeV [86] and centrality-dependent Pb-Pb collisions at $\sqrt{s_{NN}} = 2.76$ and 5.02 TeV [87], and Xe-Xe collisions at $\sqrt{s_{NN}} = 5.44$ TeV [88] from the charged particles p_T spectra, measured by the ALICE experiment at the LHC.

Figure 1 shows ξ and $F(\xi)$ as functions of final charged particle scaled pseudorapidity density at midrapidity (hereafter, multiplicity, for brevity) for pp , Xe-Xe and Pb-Pb collisions. The error in $F(\xi)$ is obtained by changing the fitting ranges of the transverse momentum spectra and is found within $\sim 3\%$. For a better comparison of pp and AA collisions, $\langle dN_{ch}/d\eta \rangle$, where N_{ch} is the measured charged particle multiplicity, is scaled by the transverse overlap area, S_{\perp} , for both pp and AA collisions. For pp collisions, multiplicity-dependent S_{\perp} is calculated using the IP-Glasma model [89]. In the case of heavy-ion collisions, the transverse overlap area is obtained using the Glauber model calculations [90]. It is observed that $F(\xi)$ falls onto a universal scaling curve for proton-proton and nucleus-nucleus collisions. Particularly, in the most central heavy-ion collisions (high number of tracks) and high-multiplicity pp collisions, $F(\xi)$ values fall in a line. This suggests that the color suppression factor is independent of collision energies and collision systems in the domain of high final state multiplicity. Further, what decides the color suppression factor is the final state multiplicity density of the system, which turns out to be the initial parton density in a system for the case of an isentropic expansion.

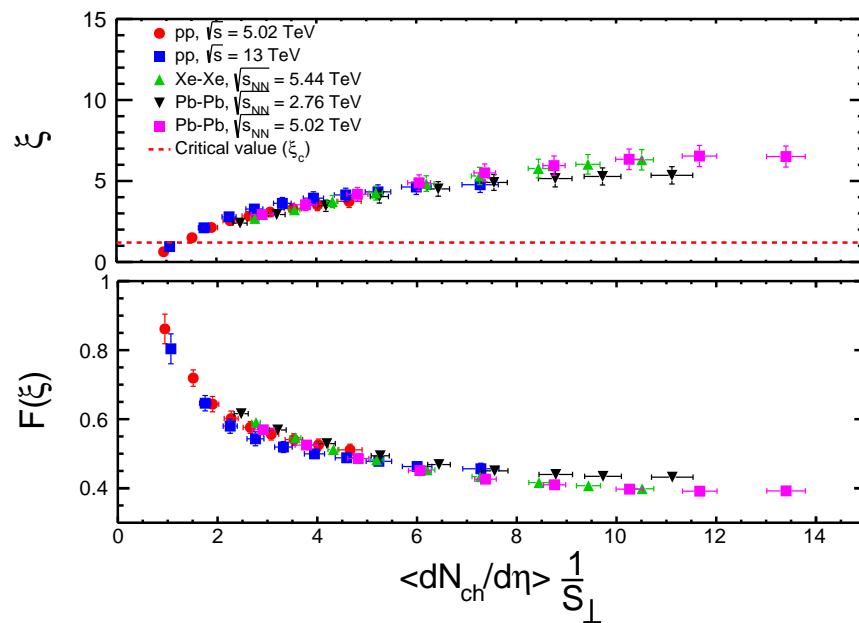


Figure 1. Percolation density parameter, ξ (upper panel), and color suppression factor, $F(\xi)$ (bottom panel), as functions of charged particle multiplicity (the pseudorapidity density at midrapidity) within $|\eta| < 0.8$ scaled with the transverse overlap area S_{\perp} in pp , Xe-Xe and Pb-Pb collisions. For pp collisions, multiplicity-dependent S_{\perp} is obtained from IP-Glasma model [89]. In case of Xe-Xe and Pb-Pb collisions, S_{\perp} values are obtained using the Glauber model [90]. See text for details.

3.1. Temperature

The connection between $F(\xi)$ and the initial percolation temperature $T(\xi)$ involves the Schwinger mechanism for particle production [63,64,67] and can be expressed as [63,68]

$$T(\xi) = \sqrt{\frac{\langle p_T^2 \rangle_1}{2F(\xi)}}. \quad (8)$$

Here, one adopts the point of view that the universal hadronization temperature, T_h , is a good measure of the upper end of the cross-over phase transition temperature [91]. The single string average transverse momentum $\langle p_T^2 \rangle_1$ is calculated at the critical percolation density parameter $\xi_c = 1.2$ with the universal hadronization temperature $T_h = 167.7 \pm 2.6$ MeV [91]. This gives $\sqrt{\langle p_T^2 \rangle_1} = 207.2 \pm 3.3$ MeV.

In this way, at $\xi_c = 1.2$, the connectivity percolation transition at $T(\xi_c)$ models the thermal deconfinement transition. The temperature obtained for most central Pb-Pb collisions at $\sqrt{s_{NN}} = 2.76$ TeV found to be of ~ 223 MeV, whereas the direct photon measurement up to $p_T < 10$ GeV/c gives the initial temperature $T_i = 297 \pm 12(\text{stat}) \pm 41(\text{syst})$ MeV for 0–20% central Pb-Pb collisions at $\sqrt{s_{NN}} = 2.76$ TeV measured by the ALICE Collaboration [92]. The measured temperature shows that the temperature obtained using Equation (8) can be termed as the temperature of the percolation cluster.

Figure 2 shows a plot of initial temperature from CSPM as a function of $\langle dN_{ch}/d\eta \rangle$ scaled by S_\perp . Temperatures from both pp and AA collisions fall on a universal curve when multiplicity is scaled by the transverse overlap area. The horizontal line at ~ 167.7 MeV is the universal hadronization temperature obtained from the systematic comparison of the statistical thermal model parametrization of hadron abundances measured in high energy e^+e^- , pp and AA collisions [91]. One can see that temperature for higher multiplicity classes in pp collisions at $\sqrt{s} = 5.02$ and 13 TeV, are higher than the hadronization temperature and similar to those observed in Xe-Xe at $\sqrt{s_{NN}} = 5.44$ TeV and Pb-Pb collisions at $\sqrt{s_{NN}} = 2.76$ and 5.02 TeV.

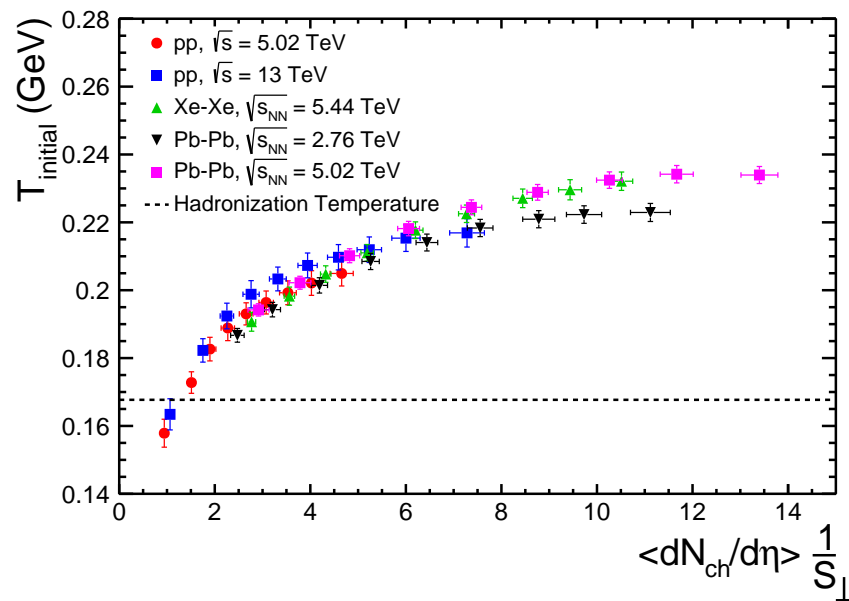


Figure 2. Initial percolation temperature vs. $\langle dN_{ch}/d\eta \rangle$, scaled by S_\perp , from pp , Pb-Pb and Xe-Xe collisions. The line ~ 167.7 MeV is the universal hadronization temperature [91].

3.2. Energy Density

The calculation of the bulk properties of hot QCD matter and characterization of the nature of the QCD phase transition is one of the most important and fundamental problems in finite-temperature QCD. The QGP, according to CSPM, is born in local thermal equilibrium because the temperature is determined at the string level. Beyond the initial temperature, $T > T_c$ the CSPM perfect fluid may expand according to Bjorken boost invariant 1-dimension hydrodynamics [93]. In this framework, the initial energy density is given by:

$$\varepsilon = \frac{3}{2} \frac{dN_{ch}}{S_N \tau_{pro}} \langle m_T \rangle, \tag{9}$$

where ε is the energy density, S_N is the transverse overlap area and τ_{pro} , the production time for a boson (gluon), is described by [94]

$$\tau_{\text{pro}} = \frac{2.405\hbar}{\langle m_T \rangle}. \tag{10}$$

Here, $m_T = \sqrt{m^2 + p_T^2}$ is the transverse mass and \hbar is the reduced Planck constant. For evaluating ε , the charged particle multiplicity (rapidity density) dN_{ch}/dy at midrapidity is used and m is taken as the pion mass (pions being the most abundant particles in the multiparticle production process such as that discussed here), which gives the lower bound of the energy density. For the estimation of $\langle m_T \rangle$, the p_T spectra of pions at different collision energies and collision species in the p_T range $0.15 \text{ GeV}/c < p_T < 1 \text{ GeV}/c$ are used.

The purpose of estimating the initial percolation temperature and the initial energy density in the framework of CSPM is to study the jet transport coefficient as a function of these global observables for different collision species and collision energies at the LHC. Let us now proceed to estimate \hat{q} in the CSPM framework.

3.3. Jet Transport Coefficient

The final state hadrons, produced in ultra-relativistic collisions at large transverse momenta, are strongly suppressed in central collisions compared to peripheral collisions. This suppression of hadrons at high p_T , which is usually referred to as jet quenching, is believed to be the result of the parton energy loss induced by multiple collisions in the strongly interacting medium. Thus, we are encouraged to study the jet transport coefficient, \hat{q} , which encodes the parton energy loss in the medium. It is also related to the p_T broadening of the energetic partons propagating inside the medium. In kinetic theory framework, \hat{q} can be estimated by the formula [95],

$$\hat{q} = \rho \int d^2q_{\perp} q_{\perp}^2 \frac{d\sigma}{d^2q_{\perp}}, \tag{11}$$

where ρ is the number density of the constituents of the medium, q_{\perp} is the transverse momentum exchange between the jet and the medium, and $d\sigma/d^2q_{\perp}$ denotes the differential scattering cross-section of the particles inside the medium.

The jet transport coefficient, \hat{q} , and the shear viscosity-to-entropy density ratio, η/s , transport parameters describing the exchange of energy and momentum between fast partons and medium, are directly related to each other as [57,96–98]

$$\frac{\eta}{s} \approx \frac{3}{2} \frac{T^3}{\hat{q}}. \tag{12}$$

Within the CSPM approach, η/s can be expressed as [64,83]

$$\frac{\eta}{s} = \frac{TL}{5(1 - e^{-\xi})}, \tag{13}$$

here L is the longitudinal extension of the string $\sim 1 \text{ fm}$ [63]. One can get final expression for jet transport coefficient from Equation (12) as:

$$\hat{q} \approx \frac{3}{2} \frac{T^3}{\eta/s} \approx \frac{15}{2} \frac{T^2(1 - e^{-\xi})}{L}. \tag{14}$$

The jet quenching parameter \hat{q} is plotted as a function of initial percolation temperature in Figure 3. Interestingly, one observes a linear increase in \hat{q} , with the increase in temperature for both pp and AA collisions. At low temperatures, the value of jet quenching parameter is around 0.02 GeV^3 . This value increases gradually and at high temperatures, it reaches the value around 0.08 GeV^3 .

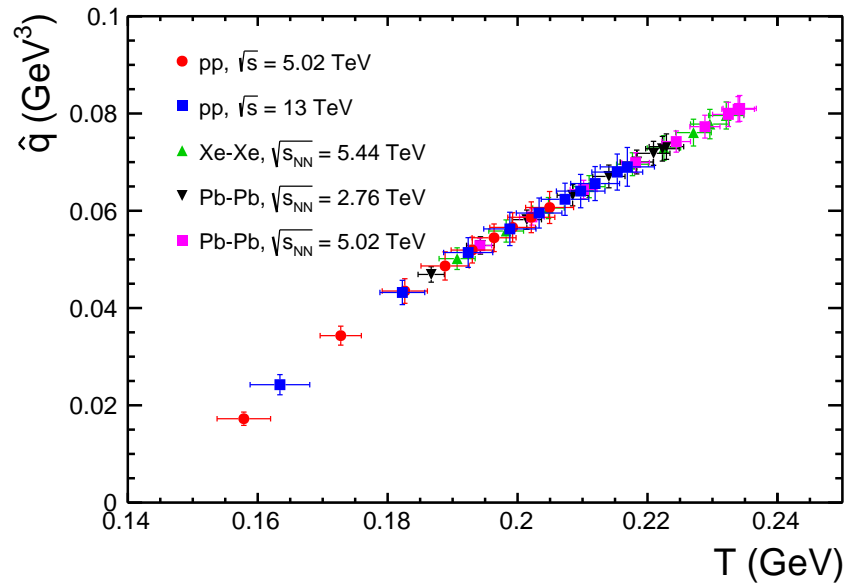


Figure 3. Jet quenching parameter, \hat{q} , as a function of temperature within the color string percolation model (CSPM) for pp collisions at $\sqrt{s} = 5.02$ and 13 TeV, Xe-Xe collisions at $\sqrt{s_{NN}} = 5.44$ TeV and Pb-Pb collisions at $\sqrt{s_{NN}} = 2.76$ and 5.02 TeV.

The JET Collaboration has also extracted \hat{q} values from five different hydrodynamic approaches with the initial temperatures of 346–373 MeV and 447–486 MeV for the most central Au-Au collisions at $\sqrt{s} = 200$ GeV at RHIC and Pb-Pb collisions at $\sqrt{s} = 2.76$ TeV at LHC, respectively [58]. The variation of \hat{q} values between different hydrodynamic models is considered as theoretical uncertainties. The scaled jet quenching parameter \hat{q}/T^3 at the highest temperatures reached in the most central Au-Au and Pb-Pb collisions are [58].

$$\frac{\hat{q}}{T^3} \approx \begin{cases} 4.6 \pm 1.2 & \text{at RHIC,} \\ 3.7 \pm 1.4 & \text{at LHC.} \end{cases}$$

The corresponding absolute values for \hat{q} for a 10 GeV quark jet are,

$$\hat{q} \approx \begin{cases} 0.23 \pm 0.05 \\ 0.37 \pm 0.13 \end{cases} \text{ GeV}^3 \text{ at } \begin{cases} T = 346\text{--}373 \text{ MeV (RHIC),} \\ T = 447\text{--}486 \text{ MeV (LHC),} \end{cases}$$

at an initial time $\tau_0 = 0.6$ fm/c. In this study, charged particle spectra are used to calculate \hat{q} within the CSPM approach, so one cannot reach the initial temperature published by the JET Collaboration. Therefore, the \hat{q} obtained is significantly smaller than the value reported by the JET Collaboration for the most central Pb-Pb collisions at $\sqrt{s} = 2.76$ TeV at the LHC.

In Figure 4, \hat{q} is plotted as a function of charged particle multiplicity scaled with transverse overlap area for pp collisions at $\sqrt{s} = 5.02$ and 13 TeV, Xe-Xe collisions at $\sqrt{s_{NN}} = 5.44$ TeV and Pb-Pb collisions at $\sqrt{s_{NN}} = 2.76$ and 5.02 TeV. One can see that \hat{q} shows a steep increase at lower charged particle multiplicities in pp collisions and gets saturated at very high multiplicity for all studied energies. This behaviour suggests that at lower multiplicities, the system is not dense enough to highly quench the partonic jets, whereas with the increase of multiplicity, the quenching of jets becomes more prominent.

The dimensionless parameter, T^3 -scaled \hat{q} is shown in Figure 5 as a function of charged particle multiplicity scaled with transverse overlap area. In the low multiplicity regime, one can see a steep increase in \hat{q}/T^3 , and after reaching a maximum at $\langle dN_{ch}/d\eta \rangle / S_{\perp} \sim 2$, it starts decreasing regardless of the collision system or collision energy. The decrease in \hat{q}/T^3 is faster in Pb-Pb and Xe-Xe as compared to the pp collisions.

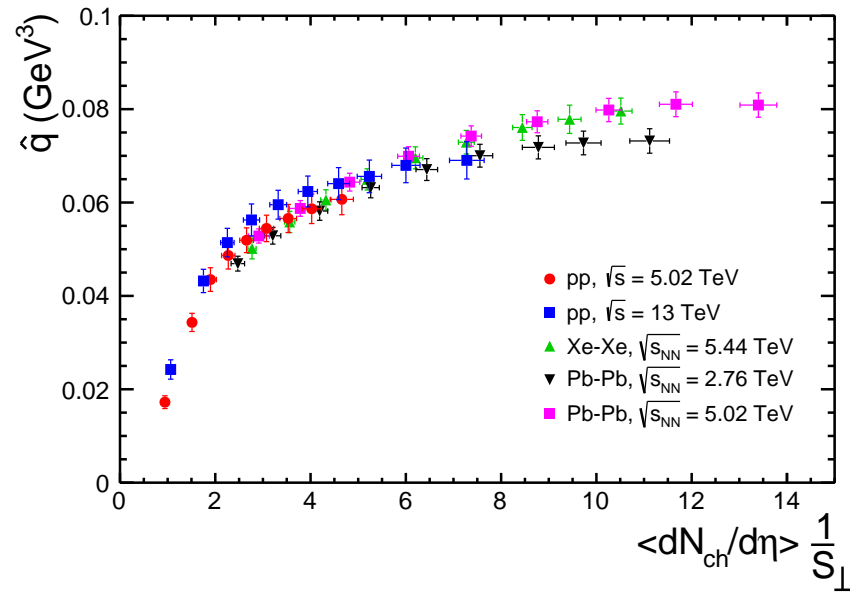


Figure 4. Jet quenching parameter, \hat{q} , as a function charged particle multiplicity scaled with transverse overlap area (S_{\perp}) within the CSPM for pp collisions at $\sqrt{s} = 5.02$ and 13 TeV, Xe-Xe collisions at $\sqrt{s_{NN}} = 5.44$ TeV and Pb-Pb collisions at $\sqrt{s_{NN}} = 2.76$ and 5.02 TeV.

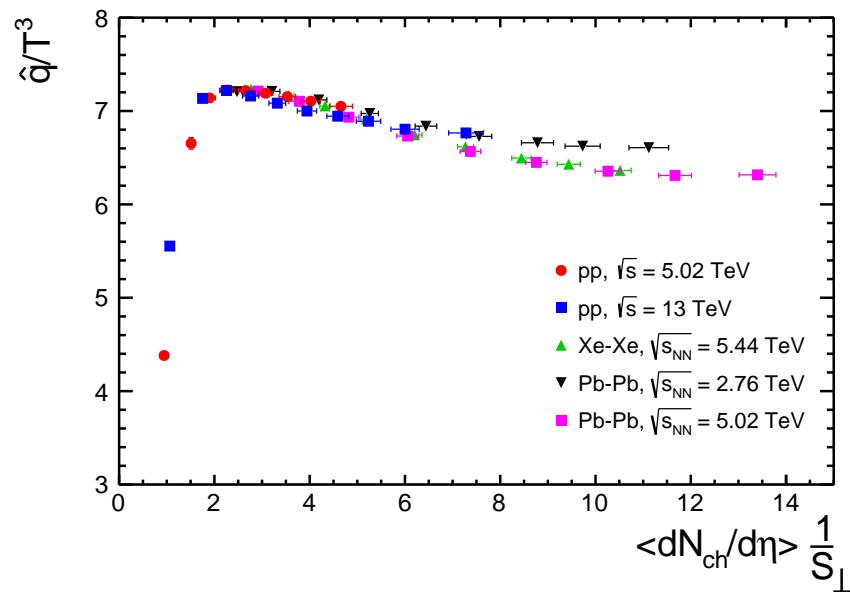


Figure 5. \hat{q}/T^3 vs. charged particle multiplicity, scaled by S_{\perp} , for pp collisions at $\sqrt{s} = 5.02$ and 13 TeV, Xe-Xe collisions at $\sqrt{s_{NN}} = 5.44$ TeV and Pb-Pb collisions at $\sqrt{s_{NN}} = 2.76$ and 5.02 TeV.

The variation of \hat{q} as a function of initial energy density is shown in Figure 6. To have a better understanding, the results obtained here are compared with that of cold nuclear matter, massless hot pion gas and ideal QGP calculations [99]. The comparison shows that the CSPM result obtained here is closer to the massless hot pion gas at low energy density. As initial energy density increases, \hat{q} values increase and then show a saturation towards heavy-ion collisions, which produce a denser medium. The saturation behaviour, observed at high energy densities suggests that \hat{q} remains unaffected after a certain energy density. Similar behaviour is observed when \hat{q} is studied as a function of multiplicity (see Figure 4). The jet energy loss inside a denser QCD medium goes towards saturation after a threshold in the final state multiplicity is reached. If one compares the behaviour of η/s as a function of T/T_c for $T > T_c$ (the domain of validity of CSPM), an increasing trend is observed, which is expected to be reflected in a reverse way in the observable \hat{q}/T^3 .

However, the interplay of higher temperature and lower η/s decides the high temperature behavior of \hat{q} as shown in Figure 6. Further, one observes the CSPM based estimations of \hat{q} showing a deviation from the ideal QGP behaviour for energy densities higher than $1 \text{ GeV}/\text{fm}^3$. This is because the ideal QGP calculations of Ref. [99], assumes ϵ/T^4 a constant value, whereas the CSPM-based estimations show an increasing trend of ϵ/T^4 towards high temperature (energy density or final state multiplicity) [84].

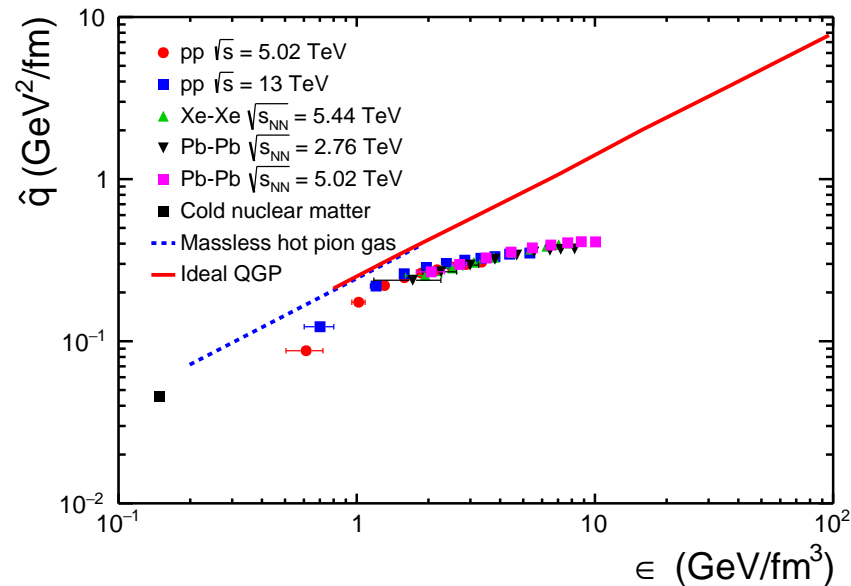


Figure 6. Jet quenching parameter, \hat{q} , as a function of initial energy density for pp collisions at $\sqrt{s} = 5.02$ and 13 TeV, Xe-Xe collisions at $\sqrt{s_{NN}} = 5.44$ TeV and Pb-Pb collisions at $\sqrt{s_{NN}} = 2.76$ and 5.02 TeV. The blue dotted line is for massless pion gas, the solid red curve is for ideal quark-gluon plasma (QGP) and the black square is for cold nuclear matter [99].

In Figure 7, \hat{q}/T^3 is plotted as a function of initial temperature. For comparison, the results obtained by the JET Collaboration are also plotted using five different theoretical models that incorporate particle energy loss in the medium. The GLV model [41–43] predicted the general form of the evolution of center-of-mass energy of the high transverse momentum pion nuclear modification factor from Super Proton Synchrotron (SPS) and RHIC to LHC energies. CUJET 1.0 explained the similarity between R_{AA} at RHIC and LHC, despite the fact that the initial QGP density in LHC almost doubles that of RHIC, by taking the effects due to multi-scale running of the QCD coupling $\alpha(Q^2)$ into account [44]. In CUJET 2.0, the CUJET 1.0 is coupled with the 2+1D (2+1 dimensional) viscous hydro fields. By taking GLV-CUJET, the JET Collaboration has estimated the scaled \hat{q} , shown by the dashed black line. The HT-BW model uses a 3+1D ideal hydrodynamics to provide the space-time evolution of the local temperature and the flow velocity in the medium along the jet propagation path in heavy-ion collisions. The result obtained from HT-BW model is represented by the blue line. The HT-M model (red line with filled circles) uses a 2+1D viscous hydrodynamic model to provide the space-time evolution of the entropy density [45–49]. The nuclear initial parton scatterings for jet production are carried out by using PYTHIA8 Monte Carlo generator in the MARTINI model [54]. This model describes the suppression of hadron spectra in heavy-ion collisions at RHIC rather well with a fixed value of the strong coupling constant. In the McGill-AMY model [52,53], the scattering and radiation processes are described by thermal QCD and hard thermal loop (HTL) effects [100] and Landau–Pomeranchuk–Migdal (LPM) interference [101]. In this approach, a set of rate equations for their momentum distributions are solved to obtain the evolution of hard jets (quarks and gluons) in the hot QCD medium. One observes that \hat{q}/T^3 obtained from the CSPM approach has a similar kind of behaviour as observed by JET Collaboration.

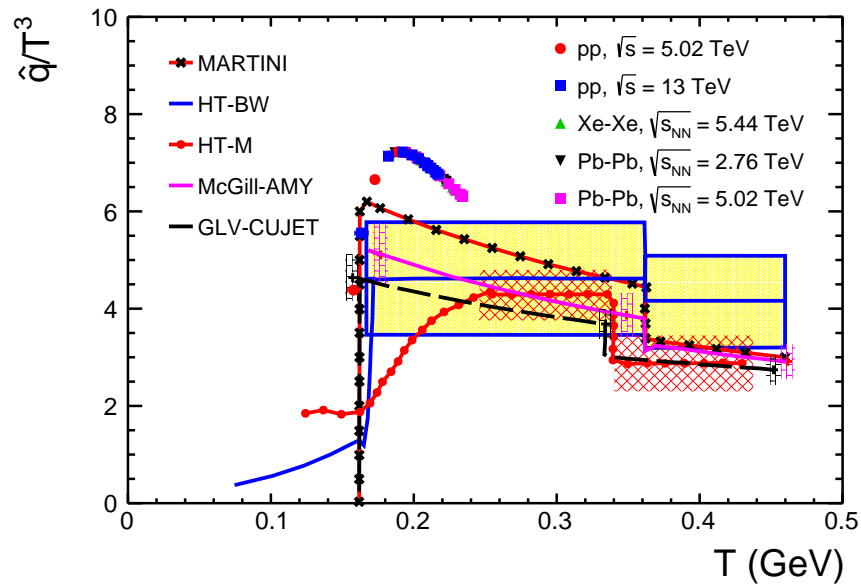


Figure 7. Scaled jet quenching parameter, \hat{q}/T^3 , as a function of initial temperature for pp collisions at $\sqrt{s} = 5.02$ and 13 TeV, Xe-Xe collisions at $\sqrt{s_{NN}} = 5.44$ TeV and Pb-Pb collisions at $\sqrt{s_{NN}} = 2.76$ and 5.02 TeV. The yellow band shows the estimated uncertainties under the high-twist high-twist Berkeley–Wuhan (HT-BW) model, whereas the red shaded region shows the corresponding uncertainty in the high-twist Majumder (HT-M) model. See text for details.

4. Conclusions

In this paper, the thermodynamic and transport properties of the matter, formed in proton-proton (pp) and heavy-ion (AA) collisions at Large Hadron Collider (LHC) energies, are studied within the framework of the color string percolation model (CSPM). The percolation density parameter is extracted by fitting transverse momentum spectra within CSPM and then initial percolation temperature (T), energy density (ϵ) and the jet transport coefficient (\hat{q}) are estimated. In the present paper, for the first time, the jet transport coefficient of produced hot QCD matter is studied within the color string percolation approach as a function of final state charged particle multiplicity (pseudorapidity density at midrapidity) at the LHC energies. It is shown that \hat{q} increases linearly with initial temperature regardless of the collision system or collision energy.

At very low multiplicity, \hat{q} shows a sharp increase and this dependence becomes weak at high multiplicity (energy density). This behaviour suggests that at lower multiplicity, the system is not dense enough to highly quench the partonic jets, whereas with the increase of multiplicity the quenching of jets becomes more prominent. At very high multiplicity (energy density), \hat{q} saturates with multiplicity (energy density). This allows us to conclude that at very high multiplicity (high energy density), \hat{q} becomes independent of final state multiplicity when scaled by the transverse overlap area of the produced fireball. Interestingly, it is found that for \hat{q} in the low energy density regime, the system behaves almost like a massless hot pion gas. The \hat{q}/T^3 , obtained from the CSPM approach as a function of temperature, T , has a similar kind of behaviour as observed by the JET Collaboration using five different theoretical models that incorporate particle energy loss in the medium.

In view of the heavy-ion-like signatures seen in TeV high-multiplicity pp collisions at the LHC energies, it would be of high interest to see the jet quenching results in such collisions to infer about the possible quark-gluon plasma droplet formation. The present study of jet transport coefficient as a function of final state multiplicity, initial temperature and energy density will pave the way for such an experimental exploration making LHC pp collisions unique.

Author Contributions: A.N.M., D.S. and R.S. have contributed to the study equally, starting from the conceptualization of the problem, methodology, paper writing and review. All authors have read and agreed to the published version of the manuscript.

Funding: This research was funded by the Hungarian National Research, Development and Innovation Office (NKFIH) under the contract numbers OTKA K135515, K123815 and NKFIH 2019-2.1.11-TET-2019-00078, 2019-2.1.11-TET-2019-00050 and DAE-BRNS Project No. 58/14/29/2019-BRNS of the Government of India.

Acknowledgments: Aditya Nath Mishra thanks the Hungarian National Research, Development and Innovation Office (NKFIH) and Wigner Scientific Computing Laboratory (WSCLAB, the former Wigner GPU Laboratory). Raghunath Sahoo acknowledges the financial supports under the CERN Scientific Associateship and the financial grants of Dept. of Atomic Energy DAE, the Board of Research in Nuclear Sciences BRNS of the Government of India.

Data Availability Statement: Not applicable.

Conflicts of Interest: The authors declare no conflict of interest.

References

1. Bjorken, J.D. *Energy Loss of Energetic Partons in Quark–Gluon Plasma: Possible Extinction of High p_T Jets in Hadron–Hadron Collisions*; Report FERMILAB-Pub-82-059-THY; Fermi National Accelerator Laboratory: Batavia, IL, USA, 1982. Available online: <https://lss.fnal.gov/archive/preprint/fermilab-pub-82-059-t.shtml> (accessed on 20 December 2021).
2. d’Enterria, D. Jet quenching. In *Landolt-Börnstein–Group. Elementary Particles, Nuclei and Atoms, 23: Relativistic Heavy Ion Physics*; Stock, R., Ed.; Springer: Berlin/Heidelberg, Germany, 2010. [CrossRef]
3. Blaizot, J.P.; McLerran, L.D. Jets in Expanding quark–gluon plasmas. *Phys. Rev. D* **1986**, *34*, 2739. [CrossRef] [PubMed]
4. Gyulassy, M.; Plumer, M. Jet quenching in dense matter. *Phys. Lett. B* **1990**, *243*, 432. [CrossRef]
5. Wang, X.N.; Gyulassy, M. Gluon shadowing and jet quenching in A + A collisions at $\sqrt{s_{NN}} = 200$ GeV. *Phys. Rev. Lett.* **1992**, *68*, 1480. [CrossRef]
6. Baier, R.; Dokshitzer, Y.L.; Peigne, S.; Schiff, D. Induced gluon radiation in a QCD medium. *Phys. Lett. B* **1995**, *345*, 277. [CrossRef]
7. Baier, R.; Dokshitzer, Y.L.; Mueller, A.H.; Peigne, S.; Schiff, D. Radiative energy loss and p_T broadening of high-energy partons in nuclei. *Nucl. Phys. B* **1997**, *484*, 265. [CrossRef]
8. Qin, G.Y.; Wang, X.N. Jet quenching in high-energy heavy-ion collisions. *Int. J. Mod. Phys. E* **2015**, *24*, 1530014. [CrossRef]
9. Gyulassy, M.; Vitev, I.; Wang, X.-N.; Zhang, B.-W. Jet quenching and radiative energy loss in dense nuclear matter. In *Quark–Gluon Plasma 3*; Hwa, R.C., Wang, X.-N., Eds.; World Scientific: Singapore, 2004; pp. 123–191. [CrossRef]
10. Adcox, K.; Adler, S.S.; Afanasiev, S.; Aidala, C.; Ajitanand, N.N.; Akiba, Y.; Al-Jamel, A.; Alexander, J.; Amirikas, R.; Aoki, K.; et al. Suppression of hadrons with large transverse momentum in central Au+Au collisions at $\sqrt{s_{NN}} = 130$ GeV. *Phys. Rev. Lett.* **2002**, *88*, 022301. [CrossRef]
11. Adler, C.; Ahammed, Z.; Allgower, C.; Amonett, J.; Anderson, B.D.; Anderson, M.; Averichev, G.S.; Balewski, J.; Barannikova, O.; Barnby, L.S.; et al. Disappearance of back-to-back high p_T hadron correlations in central Au+Au collisions at $\sqrt{s_{NN}} = 200$ GeV. *Phys. Rev. Lett.* **2003**, *90*, 082302. [CrossRef]
12. Adcox, K.; Adler, S.S.; Afanasiev, S.; Aidala, C.; Ajitanand, N.N.; Akiba, Y.; Al-Jamel, A.; Alexander, J.; Amirikas, R.; Aoki, K.; et al. Centrality dependence of the high p_T charged hadron suppression in Au+Au collisions at $\sqrt{s_{NN}} = 130$ GeV. *Phys. Lett. B* **2003**, *561*, 82. [CrossRef]
13. Adcox, K.; Adler, S.S.; Afanasiev, S.; Aidala, C.; Ajitanand, N.N.; Akiba, Y.; Al-Jamel, A.; Alexander, J.; Amirikas, R.; Aoki, K.; et al. Suppressed π^0 production at large transverse momentum in central Au+ Au collisions at $\sqrt{s_{NN}} = 200$ GeV. *Phys. Rev. Lett.* **2003**, *91*, 072301.
14. Adams, J.; Adler, C.; Aggarwal, M.M.; Ahammed, Z.; Amonett, J.; Anderson, B.D.; Anderson, M.; Arkhipkin, D.; Averichev, G.S.; Badyal, S.K.; et al. Transverse momentum and collision energy dependence of high- p_T hadron suppression in Au+Au collisions at ultrarelativistic energies. *Phys. Rev. Lett.* **2003**, *91*, 172302. [CrossRef] [PubMed]
15. Adams, J.; Adler, C.; Aggarwal, M.M.; Ahammed, Z.; Amonett, J.; Anderson, B.D.; Anderson, M.; Arkhipkin, D.; Averichev, G.S.; Badyal, S.K.; et al. Evidence from d+Au measurements for final state suppression of high- p_T hadrons in Au+Au collisions at RHIC. *Phys. Rev. Lett.* **2003**, *91*, 072304. [CrossRef] [PubMed]
16. Roland, C. Charged hadron transverse momentum distributions in Au + Au collisions at $\sqrt{s_{NN}} = 200$ GeV. *Phys. Lett. B* **2004**, *578*, 297.
17. Arsene, I.; Bearden, I.G.; Beavis, D.; Besliu, C.; Budick, B.; Boggild, H.; Chasman, C.; Christensen, C.H.; Christiansen, P.; Cibor, J.; et al. Transverse momentum spectra in Au+Au and d+Au collisions at $\sqrt{s_{NN}} = 200$ GeV and the pseudorapidity dependence of high- p_T suppression. *Phys. Rev. Lett.* **2003**, *91*, 072305. [CrossRef] [PubMed]
18. Adare, A.; Afanasiev, S.; Aidala, C.A.; Ajitanand, N.N.; Akiba, Y.; Al-Bataineh, H.; Alexander, J.; Al-Jamel, A.F.; Aoki, K.; Aphecetche, L.; et al. System size and energy dependence of jet-induced hadron pair correlation shapes in Cu+Cu and Au+Au collisions at $\sqrt{s_{NN}} = 200$ and 62.4 GeV. *Phys. Rev. Lett.* **2007**, *98*, 232302. [CrossRef] [PubMed]

19. Adcox, K.; Adler, S.S.; Afanasiev, S.; Aidala, C.; Ajitanand, N.N.; Akiba, Y.; Al-Jamel, A.; Alexander, J.; Amirikas, R.; Aoki, K.; et al. Formation of dense partonic matter in relativistic nucleus-nucleus collisions at RHIC: Experimental evaluation by the PHENIX collaboration. *Nucl. Phys. A* **2005**, *757*, 184. [[CrossRef](#)]
20. Adams, J.; Adler, C.; Aggarwal, M.M.; Ahammed, Z.; Amonett, J.; Anderson, B.D.; Anderson, M.; Arkhipkin, D.; Averichev, G.S.; Badyal, S.K.; et al. Experimental and theoretical challenges in the search for the quark gluon plasma: The STAR Collaboration's critical assessment of the evidence from RHIC collisions. *Nucl. Phys. A* **2005**, *757*, 102. [[CrossRef](#)]
21. Back, B.; Baker, M.D.; Ballintijn, M.; Barton, D.S.; Becker, B.; Betts, R.R.; Bickley, A.A.; Bindel, R.; Budzanowski, A.; Busza, W.; et al. The PHOBOS perspective on discoveries at RHIC. *Nucl. Phys. A* **2005**, *757*, 28. [[CrossRef](#)]
22. Arsene, I.; Bearden, I.G.; Beavis, D.; Besliu, C.; Budick, B.; Boggild, H.; Chasman, C.; Christensen, C.H.; Christiansen, P.; Cibor, J.; et al. Quark gluon plasma and color glass condensate at RHIC? The Perspective from the BRAHMS experiment. *Nucl. Phys. A* **2005**, *757*, 1. [[CrossRef](#)]
23. Adare, A.; Afanasiev, S.; Aidala, C.A.; Ajitanand, N.N.; Akiba, Y.; Al-Bataineh, H.; Alexander, J.; Al-Jamel, A.F.; Aoki, K.; Aphecetche, L.; et al. Quantitative constraints on the opacity of hot partonic matter from semi-inclusive single high transverse momentum pion suppression in Au+Au collisions at $\sqrt{s_{NN}} = 200$ GeV. *Phys. Rev. C* **2008**, *77*, 064907. [[CrossRef](#)]
24. Aamodt, K.; Wikne, J.; Mlynarz, J.; Lazzeroni, C.; Bruno, G.; Radomski, S.; Gheata, M.; Stefanek, G.; Piccotti, A.; Cuveland, J.; et al. Suppression of charged particle production at large transverse momentum in central Pb-Pb collisions at $\sqrt{s_{NN}} = 2.76$ TeV. *Phys. Lett. B* **2011**, *696*, 30. [[CrossRef](#)]
25. Aad, G.; Abbott, B.; Abdallah, J.; Abdelalim, A.; Abdesselam, A.; Abidinov, O.; Abi, B.; Abolins, M.; Abramowicz, H.; Abreu, H.; et al. Observation of a centrality-dependent dijet asymmetry in lead-lead collisions at $\sqrt{s_{NN}} = 2.77$ TeV with the ATLAS detector at the LHC. *Phys. Rev. Lett.* **2010**, *105*, 252303. [[CrossRef](#)] [[PubMed](#)]
26. Chatrchyan, S.; Khachatryan, V.; Sirunyan, A.M.; Tumasyan, A.; Adam, W.; Bergauer, T.; Dragicevic, M.; Erö, J.; Fabjan, C.; Friedl, M.; et al. Observation and studies of jet quenching in PbPb collisions at nucleon-nucleon center-of-mass energy = 2.76 TeV. *Phys. Rev. C* **2011**, *84*, 024906. [[CrossRef](#)]
27. Chatrchyan, S.; Khachatryan, V.; Sirunyan, A.M.; Tumasyan, A.; Adam, W.; Bergauer, T.; Dragicevic, M.; Erö, J.; Fabjan, C.; Friedl, M.; et al. Dependence on pseudorapidity and centrality of charged hadron production in PbPb collisions at a nucleon-nucleon centre-of-mass energy of 2.76 TeV. *J. High Energy Phys.* **2011**, *1108*, 141. [[CrossRef](#)]
28. Aamodt, K.; Wikne, J.; Mlynarz, J.; Lazzeroni, C.; Bruno, G.; Radomski, S.; Gheata, M.; Stefanek, G.; Piccotti, A.; Cuveland, J.; et al. Particle-yield modification in jetlike azimuthal dihadron correlations in Pb-Pb Collisions at $\sqrt{s_{NN}} = 2.76$ TeV. *Phys. Rev. Lett.* **2012**, *108*, 092301. [[CrossRef](#)]
29. Chatrchyan, S.; Khachatryan, V.; Sirunyan, A.M.; Tumasyan, A.; Adam, W.; Bergauer, T.; Dragicevic, M.; Erö, J.; Fabjan, C.; Friedl, M.; et al. Study of high- p_T charged particle suppression in PbPb compared to pp collisions at $\sqrt{s_{NN}} = 2.76$ TeV. *Eur. Phys. J. C* **2012**, *72*, 1945. [[CrossRef](#)]
30. Chatrchyan, S.; Khachatryan, V.; Sirunyan, A.M.; Tumasyan, A.; Adam, W.; Bergauer, T.; Dragicevic, M.; Erö, J.; Fabjan, C.; Friedl, M.; et al. Jet momentum dependence of jet quenching in PbPb collisions at $\sqrt{s_{NN}} = 2.76$ TeV. *Phys. Lett. B* **2012**, *712*, 176. [[CrossRef](#)]
31. Chatrchyan, S.; Khachatryan, V.; Sirunyan, A.M.; Tumasyan, A.; Adam, W.; Bergauer, T.; Dragicevic, M.; Erö, J.; Fabjan, C.; Friedl, M.; et al. Measurement of jet fragmentation into charged particles in pp and PbPb collisions at $\sqrt{s_{NN}} = 2.76$ TeV. *J. High Energy Phys.* **2012**, *1210*, 087.
32. Chatrchyan, S.; Khachatryan, V.; Sirunyan, A.M.; Tumasyan, A.; Adam, W.; Bergauer, T.; Dragicevic, M.; Erö, J.; Fabjan, C.; Friedl, M.; et al. Studies of jet quenching using isolated-photon+jet correlations in PbPb and pp collisions at $\sqrt{s_{NN}} = 2.76$ TeV. *Phys. Lett. B* **2013**, *718*, 773. [[CrossRef](#)]
33. Aad, G.; Abbott, B.; Abdallah, J.; Abdelalim, A.; Abdesselam, A.; Abidinov, O.; Abi, B.; Abolins, M.; Abramowicz, H.; Abreu, H.; et al. Measurement of the jet radius and transverse momentum dependence of inclusive jet suppression in lead-lead collisions at $\sqrt{s_{NN}} = 2.76$ TeV with the ATLAS detector. *Phys. Lett. B* **2013**, *719*, 220. [[CrossRef](#)]
34. Chatrchyan, S.; Khachatryan, V.; Sirunyan, A.M.; Tumasyan, A.; Adam, W.; Bergauer, T.; Dragicevic, M.; Erö, J.; Fabjan, C.; Friedl, M.; et al. Evidence of b-jet quenching in PbPb collisions at $\sqrt{s_{NN}} = 2.76$ TeV. *Phys. Rev. Lett.* **2014**, *113*, 132301. [[CrossRef](#)] [[PubMed](#)]
35. CMS Collaboration. Modification of jet shapes in PbPb collisions at $\sqrt{s_{NN}} = 2.76$ TeV. *Phys. Lett. B* **2014**, *730*, 243. [[CrossRef](#)]
36. CMS Collaboration. Measurement of jet fragmentation in PbPb and pp collisions at $\sqrt{s_{NN}} = 2.76$ TeV. *Phys. Rev. C* **2014**, *90*, 024908. [[CrossRef](#)]
37. Aad, G.; Abbott, B.; Abdallah, J.; Abdelalim, A.; Abdesselam, A.; Abidinov, O.; Abi, B.; Abolins, M.; Abramowicz, H.; Abreu, H.; et al. Measurement of inclusive jet charged-particle fragmentation functions in Pb+Pb collisions at $\sqrt{s_{NN}} = 2.76$ TeV with the ATLAS detector. *Phys. Lett. B* **2014**, *739*, 320. [[CrossRef](#)]
38. Aad, G.; Abbott, B.; Abdallah, J.; Abdelalim, A.; Abdesselam, A.; Abidinov, O.; Abi, B.; Abolins, M.; Abramowicz, H.; Abreu, H.; et al. Measurements of the nuclear modification factor for jets in Pb+Pb collisions at $\sqrt{s_{NN}} = 2.76$ TeV with the ATLAS detector. *Phys. Rev. Lett.* **2015**, *114*, 072302. [[CrossRef](#)] [[PubMed](#)]
39. Zakharov, B. Fully quantum treatment of the Landau-Pomeranchuk-Migdal effect in QED and QCD. *JETP Lett.* **1996**, *63*, 952. [[CrossRef](#)]

40. Baier, R.; Dokshitzer, Y.L.; Mueller, A.H.; Peigne, S.; Schiff, D. Radiative energy loss of high-energy quarks and gluons in a finite volume quark-gluon plasma. *Nucl. Phys. B* **1997**, *483*, 291. [[CrossRef](#)]
41. Gyulassy, M.; Levai, P.; Vitev, I. Jet quenching in thin quark gluon plasmas. 1. Formalism. *Nucl. Phys. B* **2000**, *571*, 197. [[CrossRef](#)]
42. Gyulassy, M.; Levai, P.; Vitev, I. Non-Abelian energy loss at finite opacity. *Phys. Rev. Lett.* **2000**, *85*, 5535. [[CrossRef](#)]
43. Gyulassy, M.; Levai, P.; Vitev, I. Reaction operator approach to nonAbelian energy loss. *Nucl. Phys. B* **2001**, *594*, 371. [[CrossRef](#)]
44. Buzzatti, A.; Gyulassy, M. Jet flavor tomography of quark gluon plasmas at RHIC and LHC. *Phys. Rev. Lett.* **2012**, *108*, 022301. [[CrossRef](#)] [[PubMed](#)]
45. Guo, X.F.; Wang, X.N. Multiple scattering, parton energy loss and modified fragmentation functions in deeply inelastic e A scattering. *Phys. Rev. Lett.* **2000**, *85*, 3591. [[CrossRef](#)] [[PubMed](#)]
46. Wang, X.-N.; Guo, X.-F. Multiple parton scattering in nuclei: Parton energy loss. *Nucl. Phys. A* **2001**, *696*, 788. [[CrossRef](#)]
47. Chen, X.F.; Hirano, T.; Wang, E.; Wang, X.N.; Zhang, H. Suppression of high p_T hadrons in Pb+Pb Collisions at LHC. *Phys. Rev. C* **2011**, *84*, 034902. [[CrossRef](#)]
48. Majumder, A. Hard collinear gluon radiation and multiple scattering in a medium. *Phys. Rev. D* **2012**, *85*, 014023. [[CrossRef](#)]
49. Vitev, I.; Zhang, B.W. Jet tomography of high-energy nucleus-nucleus collisions at next-to-leading order. *Phys. Rev. Lett.* **2010**, *104*, 132001. [[CrossRef](#)] [[PubMed](#)]
50. Wiedemann, U.A. Gluon radiation off hard quarks in a nuclear environment: Opacity expansion. *Nucl. Phys. B* **2000**, *588*, 303. [[CrossRef](#)]
51. Wiedemann, U.A. Jet quenching versus jet enhancement: A quantitative study of the BDMPS-Z gluon radiation spectrum. *Nucl. Phys.* **2001**, *690*, 731. [[CrossRef](#)]
52. Arnold, P.B.; Moore, G.D.; Yaffe, L.G. Photon emission from ultrarelativistic plasmas. *J. High Energy Phys.* **2001**, *11*, 057. [[CrossRef](#)]
53. Arnold, P.B.; Moore, G.D.; Yaffe, L.G. Photon and gluon emission in relativistic plasmas. *J. High Energy Phys.* **2002**, *6*, 030. [[CrossRef](#)]
54. Schenke, B.; Gale, C.; Jeon, S. MARTINI: An Event generator for relativistic heavy-ion collisions. *Phys. Rev. C* **2009**, *80*, 054913. [[CrossRef](#)]
55. Fochler, O.; Xu, Z.; Greiner, C. Energy loss in a partonic transport model including bremsstrahlung processes. *Phys. Rev. C* **2010**, *82*, 024907. [[CrossRef](#)]
56. He, Y.; Luo, T.; Wang, X.N.; Zhu, Y. Linear Boltzmann transport for jet propagation in the quark-gluon plasma: Elastic processes and medium recoil. *Phys. Rev. C* **2015**, *91*, 054908; Erratum in *Phys. Rev. C* **2018**, *97*, 019902. [[CrossRef](#)]
57. Casalderrey-Solana, J.; Wang, X.N. Energy dependence of jet transport parameter and parton saturation in Quark-Gluon plasma. *Phys. Rev. C* **2008**, *77*, 024902. [[CrossRef](#)]
58. Burke, K.M.; Buzzatti, A.; Chang, N.; Gale, C.; Gyulassy, M.; Heinz, U.; Jeon, S.; Majumder, A.; Muller, B.; Qin, G.Y.; et al. Extracting the jet transport coefficient from jet quenching in high-energy heavy-ion collisions. *Phys. Rev. C* **2014**, *90*, 014909. [[CrossRef](#)]
59. Armesto, N.; Braun, M.A.; Ferreira, E.G.; Pajares, C. Percolation approach to quark-gluon plasma and J/ψ suppression. *Phys. Rev. Lett.* **1996**, *77*, 3736. [[CrossRef](#)] [[PubMed](#)]
60. Braun, M.A.; Pajares, C. Implications of percolation of color strings on multiplicities, correlations and the transverse momentum. *Eur. Phys. J. C* **2000**, *16*, 349. [[CrossRef](#)]
61. Braun, M.A.; Pajares, C. Transverse momentum distributions and their forward backward correlations in the percolating color string approach. *Phys. Rev. Lett.* **2000**, *85*, 4864. [[CrossRef](#)]
62. Braun, M.A.; del Moral, F.; Pajares, C. Percolation of strings and the first RHIC data on multiplicity and transverse momentum distributions. *Phys. Rev. C* **2002**, *65*, 024907. [[CrossRef](#)]
63. Dias de Deus, J.; Pajares, C. Percolation of color sources and critical temperature. *Phys. Lett. B* **2006**, *642*, 455. [[CrossRef](#)]
64. Braun, M.A.; Dias de Deus, J.; Hirsch, A.S.; Pajares, C.; Scharenberg, R.P.; Srivastava, B.K. De-confinement and clustering of color sources in nuclear collisions. *Phys. Rep.* **2015**, *599*, 1. [[CrossRef](#)]
65. de Deus, J.D.; Pajares, C. String percolation and the glasma. *Phys. Lett. B* **2011**, *695*, 211. [[CrossRef](#)]
66. Braun, M.A.; del Moral, F.; Pajares, C. Centrality dependence of the multiplicity and transverse momentum distributions at RHIC and LHC and the percolation of strings. *Nucl. Phys. A* **2003**, *715*, 791. [[CrossRef](#)]
67. Schwinger, J. Gauge invariance and mass. II. *Phys. Rev.* **1962**, *128*, 2425. [[CrossRef](#)]
68. Scharenberg, R.P.; Srivastava, B.K.; Hirsch, A.S. Percolation of color sources and the determination of the equation of state of the quark-gluon plasma (QGP) produced in central Au-Au collisions at $\sqrt{s_{NN}} = 200$ GeV. *Eur. Phys. J. C* **2011**, *71*, 1510. [[CrossRef](#)]
69. Isichenko, M.B. Percolation, statistical topography, and transport in random media. *Rev. Mod. Phys.* **1992**, *64*, 961. [[CrossRef](#)]
70. Satz, H. Color deconfinement in nuclear collisions. *Rep. Prog. Phys.* **2000**, *63*, 1511. [[CrossRef](#)]
71. Mishra, A.N.; Caulte, E.; Paić, G.; Pajares, C.; Scharenberg, R.P.; Srivastava, B.K. ALICE data in the framework of the color string percolation model. *PoS* **2019**. [[CrossRef](#)]
72. Cunqueiro, L.; Dias de Deus, J.; Pajares, C. Nuclear like effects in proton-proton collisions at high energy. *Eur. Phys. J. C* **2010**, *65*, 423. [[CrossRef](#)]
73. Andres, C.; Moscoso, A.; Pajares, C. Onset of the ridge structure in AA, pA, and pp collisions. *Phys. Rev. C* **2014**, *90*, 054902. [[CrossRef](#)]

74. Scharenberg, R.P. The QGP equation of state by measuring the color suppression factor at RHIC and LHC energies. *PoS* **2013**. [[CrossRef](#)]
75. Dias de Deus, J.; Hirsch, A.S.; Pajares, C.; Scharenberg, R.P.; Srivastava, B.K. Clustering of color sources and the shear viscosity of the QGP in heavy ion collisions at RHIC and LHC energies. *Eur. Phys. J. C* **2012**, *72*, 2123. [[CrossRef](#)]
76. Srivastava, B.K. Percolation approach to initial stage effects in high energy collisions. *Nucl. Phys. A* **2014**, *926*, 142. [[CrossRef](#)]
77. Dias de Deus, J.; Hirsch, A.S.; Pajares, C.; Scharenberg, R.P.; Srivastava, B.K. Transport coefficient to trace anomaly in the clustering of color sources approach. *Phys. Rev. C* **2016**, *93*, 024915. [[CrossRef](#)]
78. Sahoo, P.; De, S.; Tiwari, S.K.; Sahoo, R. Energy and centrality dependent study of deconfinement phase transition in a color string percolation approach at RHIC energies. *Eur. Phys. J. A* **2018**, *54*, 136. [[CrossRef](#)]
79. Sahoo, P.; Tiwari, S.K.; De, S.; Sahoo, R.; Scharenberg, R.P.; Srivastava, B.K. Thermodynamic and transport properties in Au + Au collisions at RHIC energies from the clustering of color strings. *Mod. Phys. Lett. A* **2019**, *34*, 1950034. [[CrossRef](#)]
80. Sahoo, P.; Sahoo, R.; Tiwari, S.K. Wiedemann-Franz law for hot QCD matter in a color string percolation scenario. *Phys. Rev. D* **2019**, *100*, 051503. [[CrossRef](#)]
81. Sahoo, P.; Tiwari, S.K.; Sahoo, R. Electrical conductivity of hot and dense QCD matter created in heavy-ion collisions: A color string percolation approach. *Phys. Rev. D* **2018**, *98*, 054005. [[CrossRef](#)]
82. Sahu, D.; Tripathy, S.; Sahoo, R.; Tiwari, S.K. Formation of a perfect fluid in pp p-Pb, Xe-Xe and Pb-Pb collisions at the Large Hadron Collider energies. *arXiv* **2001**, arXiv:2001.01252.
83. Sahu, D.; Sahoo, R. Thermodynamic and transport properties of matter formed in pp, p-Pb, Xe-Xe and Pb-Pb collisions at the Large Hadron Collider using color string percolation model. *J. Phys. G* **2021**, *48*, 125104. [[CrossRef](#)]
84. Mishra, A.N.; Paić, G.; Pajares, C.; Scharenberg, R.P.; Srivastava, B.K. Deconfinement and degrees of freedom in pp and A-A collisions at LHC energies. *Eur. Phys. J. A* **2021**, *57*, 245. [[CrossRef](#)]
85. McLerran, L.; Venugopalan, R. Computing quark and gluon distribution functions for very large nuclei. *Phys. Rev. D* **1994**, *49*, 2233. [[CrossRef](#)] [[PubMed](#)]
86. Acharya, S.; Adamová, D.; Adhya, S.P.; Adler, A.; Adolfsson, J.; Aggarwal, M.M.; Aglieri Rinella, G.; Agnello, M.; Agrawal, N.; Ahammed, Z.; et al. Charged-particle production as a function of multiplicity and transverse sphericity in pp collisions at $\sqrt{s} = 5.02$ and 13 TeV. *Eur. Phys. J. C* **2019**, *79*, 857. [[CrossRef](#)]
87. Acharya, S.; Adamová, D.; Adhya, S.P.; Adler, A.; Adolfsson, J.; Aggarwal, M.M.; Aglieri Rinella, G.; Agnello, M.; Agrawal, N.; Ahammed, Z.; et al. Transverse momentum spectra and nuclear modification factors of charged particles in pp, p-Pb and Pb-Pb collisions at the LHC. *J. High Energy Phys.* **2018**, *11*, 013.
88. Acharya, S.; Acosta, F.T.; Adamová, D.; Adolfsson, J.; Aggarwal, M.M.; Aglieri Rinella, G.; Agnello, M.; Agrawal, N.; Ahammed, Z.; Ahn, S.U.; et al. Transverse momentum spectra and nuclear modification factors of charged particles in Xe-Xe collisions at $\sqrt{s_{NN}} = 5.44$ TeV. *Phys. Lett. B* **2019**, *788*, 166. [[CrossRef](#)]
89. McLerran, L.; Praszalowicz, M.; Schenke, B. Transverse momentum of protons, pions and Kaons in high multiplicity pp and pA collisions: Evidence for the color glass condensate? *Nucl. Phys. A* **2013**, *916*, 210. [[CrossRef](#)]
90. Loizides, C. Glauber modeling of high-energy nuclear collisions at the subnucleon level. *Phys. Rev. C* **2016**, *94*, 024914. [[CrossRef](#)]
91. Becattini, F.; Castorina, P.; Milov, A.; Satz, H. A Comparative analysis of statistical hadron production. *Eur. Phys. J. C* **2010**, *66*, 377. [[CrossRef](#)]
92. Acharya, S.; Acosta, F.T.; Adamová, D.; Adolfsson, J.; Aggarwal, M.M.; Aglieri Rinella, G.; Agnello, M.; Agrawal, N.; Ahammed, Z.; Ahn, S.U.; et al. Direct photon production in Pb-Pb collisions at $\sqrt{s_{NN}} = 2.76$ TeV. *Phys. Lett. B* **2016**, *754*, 235.
93. Bjorken, J.D. Highly relativistic nucleus-nucleus collisions: The central rapidity region. *Phys. Rev. D* **1983**, *27*, 140. [[CrossRef](#)]
94. Wong, C.Y. *Introduction to High Energy Heavy Ion Collisions*; World Scientific: Singapore, 1994. [[CrossRef](#)]
95. Baier, R.; Mehtar-Tani, Y. Jet quenching and broadening: The Transport coefficient \hat{q} in an anisotropic plasma. *Phys. Rev. C* **2008**, *78*, 064906. [[CrossRef](#)]
96. Liu, H.; Rajagopal, K.; Wiedemann, U.A. Calculating the jet quenching parameter from AdS/CFT. *Phys. Rev. Lett.* **2006**, *97*, 182301. [[CrossRef](#)] [[PubMed](#)]
97. Majumder, A.; Muller, B.; Wang, X.N. Small shear viscosity of a quark-gluon plasma implies strong jet quenching. *Phys. Rev. Lett.* **2007**, *99*, 192301. [[CrossRef](#)] [[PubMed](#)]
98. Xu, J. Shear viscosity of nuclear matter. *Nucl. Sci. Tech.* **2013**, *24*, 50514.
99. Baier, R. Jet quenching. *Nucl. Phys. A* **2003**, *715*, 209. [[CrossRef](#)]
100. Su, N. A brief overview of hard-thermal-loop perturbation theory. *Commun. Theor. Phys.* **2012**, *57*, 409. [[CrossRef](#)]
101. Baier, R.; Dokshitzer, Y.L.; Mueller, A.H.; Peigne, S.; Peigne, S.; Schiff, D. The Landau-Pomeranchuk-Migdal effect in QED. *Nucl. Phys. B* **1996**, *478*, 577. [[CrossRef](#)]